ANDRZEJ PYTLIK [1*], MARIUSZ SZOT [1]

COMPARATIVE TESTING OF CABLE BOLT AND WIRE ROPE LACING RESISTANCE TO STATIC AND DYNAMIC LOADS

The conduction of mining activity under the conditions of rock bursts and rock mass tremors means that designers often utilise support systems comprising various configurations of steel arch, rock bolt and surface support. Particularly difficult geological and mining conditions, when wire mesh does not provide sufficient dynamic resistance, it requires an additional reinforcement with wire rope lacing in the form of steel ropes installed between the bolt ends and fixed to them by means of various rope clamps (e.g. u-bolt clamps). Bench tests were conducted to compare the strength of wire ropes under static and dynamic loading. The tests involved wire ropes with an internal diameter of Ø15.7 mm. Tests under static loading demonstrated that the cable bolts transferred a maximum force $F_{smax} = 289.0$ kN without failure, while the energy absorbed until failure was $E_{1s} = 16.6$ kJ. A comparative test result analysis for the wire ropes used in the bolt designs revealed that the influence of dynamic loading forces has a significant effect on reducing the rope load capacity, which results in the brittle cracking of the wires in the rope. Although the average dynamic force leading to wire rope failure $F_{dmax} = 279.1$ kN is comparable to the minimum static force $F_{min} = 279$ kN defined in the relevant standard, the average energy E_{1d} absorbed by the cable bolt until failure is **48% lower** than the energy E_{1s} determined for wire rope failure under static loading. Furthermore, cable bolt failure under dynamic loading occurred at an impact velocity of the combined ram and crosshead masses ranging within $v_p = 1.4$-1.5 m/s.

Keywords: Rock support; cable bolts; wire rope lacing; rock bursts; drop weight impact method

1. Introduction

Various types of support systems are used to secure mine gallery and chamber workings from the influence of static and dynamic loads exerted by the rock mass: rock bolt and surface support [1-27] as well as steel arch and mixed support [28-38].

1   GIG – NATIONAL RESEARCH INSTITUTE, PLAC GWARKÓW 1, 40-166 KATOWICE, POLAND

*   Corresponding author: apytlik@gig.eu
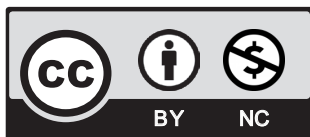
The conduction of extraction under difficult geological and mining conditions frequently accompanied by rock bursts and rock mass tremors means that designers often utilise mixed support systems comprising various configurations of rock support. The mixed cable bolt and wire rope support [3,16] used in mines in the USA is one example of such. In this system, a wire rope is installed at the working roof between cable bolts, thereby putting the rope at risk of loads exerted by the rock mass in a direction transverse to its longitudinal axis, which does not constitute its typical mode of operation. The primary advantage of this solution is the elimination of the necessity to install additional roof support measures in the working, which otherwise often constitute an obstacle for mine transport. Another example is found in a rock bolt support system combined with surface support in the form of wire mesh (welded or twisted diamond) spread between the bolts over the working outline and further reinforced with wire rope lacing, as used in mines in the RSA. An example diagram of a working secured by means of a support system comprising cable bolts and wire mesh reinforced with wire rope lacing is presented in Fig. 1.
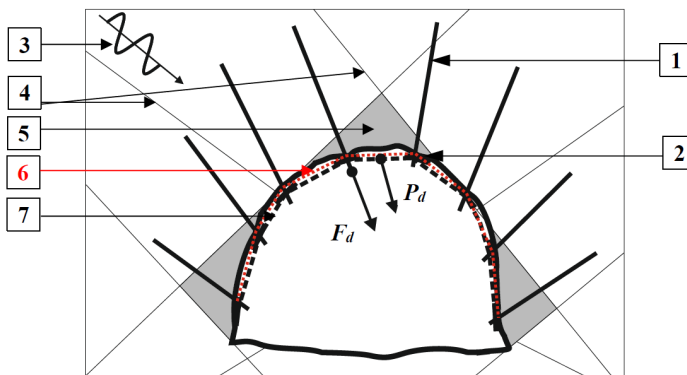

Fig. 1. Example diagram of a working with rock bolt support reinforced with wire rope lacing:
F_d – dynamic tensile force exerted on the cable bolt; P_d – dynamic force loading the wire rope lacing;
1 – cable bolt; 2 – bolt face plate; 3 – seismic wave pulse; 4 – planes of discontinuity; 5 – rock block capable of penetrating into the working; 6 – wire mesh over the working outline; 7 – wire rope lacing fixed to the cable bolt ends by means of u-bolt rope clamps

Tests conducted by the Safety in Mines Research Advisory Committee of South Africa and published in the GAP 221 [39] and GAP 423 [40] reports demonstrated that one of the basic parameters for evaluating the rock bolt support under dynamic loading is the value of the energy absorbed by its elements as well as the bolt yield. Also, according to the general principles of support system design for conditions at risk of rock bursts, as formulated by Kaiser and Cai [41], the basic assessment criterion for bolts intended for application under the conditions of dynamic loads, other than the bolt yield and load capacity, is the value of the energy absorbed by the bolts. At the same time, all the individual elements of the support system must be compatible with each other and interact to create an optimal support system, securing the working from the effects of rock bursts.

The primary bolt element responsible for assuming the load and absorbing the impact energy is the wire rope in the cable bolts and rope bolts (formed as a strand of wires or bars), or bars typically in the form of rods (metal, wooden, plastic or composite), or tubes anchored in the rock

mass by means of mechanical elements (e.g. expanding or wedge heads), cementitious materials or grouts pumped into the (anchoring) borehole or applied in the form of cement or resin charges.

Cable bolts (whose test results are presented in this publication) and rope bolts differ from other types of bolts in that their primary intended application is long bolting in major workings found in hard coal mines, metal ore mines and tunnels, as well as securing, e.g. preparatory workings in zones of mining influence or securing workings under difficult geological and mining conditions. The term "long bolting" [42] refers to using bolts with a length greater than the working height. Cable and rope bolts are characterised by a high load capacity and the possibility of pre-tensioning, which increases the self-supporting capacity of the rock mass adjacent to the working. The ropes of these bolts are typically in the form of wire strands made of high-strength steel, gripped in a rope socket (with an external thread) or by a barrel and wedge clamp.

Part of the impact energy is also absorbed by steel mesh [11,20,43-47] spread between the bolts over the working outline, which all combine into a rock bolt and surface support system for securing the working [18]. Surface support systems are primarily significant due to their close interaction with rock bolt support systems, often forming mixed yielding rock bolt and surface support systems with the capability to absorb energy not only under static loading but also during the impact of rock flows as a result of a rock burst. The surface support systems most commonly applied in practice include:
- steel mesh,
- steel straps,
- wire rope lacing,
- reinforced and regular concrete and shotcrete,
- thin spray-on liners (TSL).

Steel mesh is used in combination with steel arch, rock bolt as well as mixed support. However, compared to other load-bearing support elements [20], steel wire mesh failure typically occurs at a relatively minor impact energy, as determined based on laboratory testing performed in numerous research centres, for example:
- 1.18 kJ/m^2 – Villaescusa's [49] studies conducted at WASM (*Western Australia School of Mines*),
- 4.2 kJ when loaded by a beam and 3 kJ when loaded by a spherical cap (0.5 m-wide mesh installed on ŁP support frame sections with 1.0 m spacing) – per testing conducted at GIG, supplemented with mesh designs [50] used in the recent years in Polish hard coal mines: 2.644-5.286 kJ/m^2 [18],
- 1.5-4 kJ/m^2 – per Kaiser's studies [43],
- 10 kJ/m^2 – per Stacey's studies [18].

Additional wire rope lacing is often used to improve the impact strength of wire mesh, which is fixed to the bolt ends with the purpose of supporting the mesh and preventing the loss of its continuity. The wire ropes are typically coupled using barrel and wedge clamps (composed of a tapered socket and 2-part or 3-part wedges) [51] or various types of bolt clamps – e.g. u-bolt clamps.

Requirements for wire mesh are defined in standards such as the following: PN-G-15050:2018-01 [50], ASTM F432-19 [52], CAN/CSA-M430-90 [53]. However, these standards concern mesh testing under static loading. Dynamic testing of steel mesh and wire rope lacing is not standardised, though it is nevertheless performed in laboratories such as: *the Western Australian School of Mines* (Australia), *the Safety in Mines Research Advisory Committee* (South Africa)

and *the Central Mining Institute* (Poland), where it is typically conducted by way of a panel test in drop weight impact test facilities.

The main goal of this paper is to present and compare the values of forces resulting in rope failure at various load directions and rates as well as at various energy absorbed by the ropes until their failure. Knowledge of the mechanical properties of steel ropes used as bolt and wire rope lacing elements, determined based on strength tests, is essential to mine support designers in the process of support selection for operation under the conditions of increased static loads originating from the rock mass and dynamic loads exerted on the support elements as a result of tremors and rock bursts. Cable bolt users should consider that the rope load and energy absorption capacity may decrease when applied under conditions at risk of rock bursts. A reduction in the strength of ropes used in wire rope lacing should also be factored in due to the influence of shearing forces generated, e.g. by rock loading the wire ropes perpendicularly to their axis.

Typically, static loads increase slowly in structures and generate no inertial force in their construction, whereas the influence of dynamic loads on structures generates significant enough accelerations of their elements to make inertial forces play a significant role that cannot be disregarded during structural calculations. Dynamic loads exerted on a construction subject it to time-variable (i.e. dynamic) internal forces and displacements. Even a relatively low dynamic force applied to structural elements can result in the generation of significantly greater internal forces and displacements than a force applied in a static manner [54].

This paper presents the results of the comparative bench testing of wire rope resistance to static and dynamic loading. The tests of cable bolt resistance to static loads were performed under tensile loading, whereas the wire rope lacing was tested under tensile loads exerted on the wire rope as a result of its deflection by the influence of a transverse force applied to its longitudinal axis. Such a manner of wire rope lacing testing simulates the load exerted by the rock mass, whereas contact loading is simulated by a steel cylinder. Thermal imaging measurements at the contact point of the element loading the wire rope were carried out during the static tensile testing of the wire rope lacing in order to observe the stress distribution at the contact point and to compare it to the temperature distribution in the remaining part of the rope. Experience obtained from the work on steel rope thermoelasticity [55] as performed at GIG was used in the thermal imaging measurements. The tests of cable bolt and wire rope lacing resistance to dynamic loading were performed at a drop weight testing facility using a ram with a mass of 4000 kg and a crosshead with a mass of 3300 kg that exerted static loading on the cable bolt.

2. Materials and methods

The tests encompassed $1 \times 7 (1 + 6)$ wire ropes with an external diameter of Ø15.7 mm and a strength class of 1860 MPa, utilised in constructions prestressed per standards PN-EN ISO 15630-3 [56] and prEN 10138-3 [57], with their cross-section presented as a diagram in Fig. 2 and their structural and mechanical properties compiled in TABLE 1. These wire ropes were used to produce test samples of cable bolts and wire rope lacing.

As per the relevant standard [58], the length of spiral rope samples (with the exception of rope ends) with a diameter of 6 mm $< D \le 20$ mm that are subjected to tensile testing should be at least $L_0 = 1000$ mm. The length $L_0 = 1320$ mm of the wire ropes used during the wire rope lacing tests under loads perpendicular to their axis was selected with the intention to acquire the closest representation of the diagonal dimension of a 1×1 m square of a typical bolting grid.
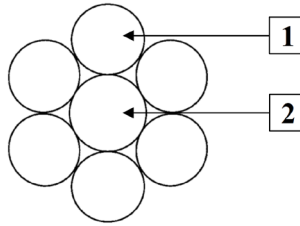
Fig. 2. Cross-section diagram of a 1×7 $(1 + 6)$ spiral wire rope with a diameter of Ø15.7 mm:
1 – strand wires, 2 – core wire

TABLE 1

Structural and mechanical properties of 1×7 $(1 + 6)$ spiral wire ropes with an external
diameter of Ø15.7 mm

Rope structure	Rope diameter D, mm	Metallic cross-section A, mm²	Strength R_m, MPa	Minimum breaking force F_{min}, kN
Spiral: 1×5.35 mm core wire 6×5.20 mm strand wires	15.7	150.0	1860	279.0

The tensile tests of the bolts and lacing under static loading were performed using the ZMLK 500 (maximum range: 5 MN, maximum expanded uncertainty over the entire measuring range: 0.72%) and AJ AMSLER (maximum range: 5 MN, maximum expanded uncertainty over the entire measuring range: 0.33%) universal testing machines. Tests of 16 bolts were performed according to the load case presented in Fig. 3a in the ZMLK 500 testing machine. The tests of cable bolts with a length $L_0 = 1050$ mm (wire rope length between the internal surfaces of the wedges in an MK4 barrel and wedge clamp) under static loading involved measuring the force loading the rope F_s as well as the rope elongation ΔL. The MK4 wedge clamps find common application for prestressing concrete constructions [57,59].

As per the relevant standard [58], the static load exerted on the rope was increased gradually, starting from zero and rising up to 80% of the minimum rope breaking force F_{min}. After achieving 80% of F_{min}, the successive load increment was no greater than 0.5% F_{min} per second, which corresponded to $v_{s\,max} = 1.395$ kN/s.

The energy absorbed by a wire rope E_{1s} until the failure of the first wire is calculated using the following formula:

$$E_{1s} = \int_0^{L_{max}} F_s(L)\, dL,\ [\text{kJ}] \tag{1}$$

where: ΔL_{max} – maximum rope elongation at failure, mm.

The energy absorbed by the wire ropes was calculated using OriginPro 6.1 by Microcal Software, Inc., which also made it possible to produce all the charts of loading as a function of displacement and time that were determined based on the measurements and included in this paper. The validity of the calculations was also confirmed when analysing the courses of loading

as a function of displacement and time in the HBM CATMAN software, which also served to register the measurement data, and when calculating the energy in EXCEL by means of numerical integration formulas via the trapezoidal rule.

The wire rope lacing tests were performed in the AJ AMSLER testing machine using a frame (10) made specifically for this purpose, according to the load case in Fig. 3b. A total of 8 pieces of wire rope lacing were subjected to testing.
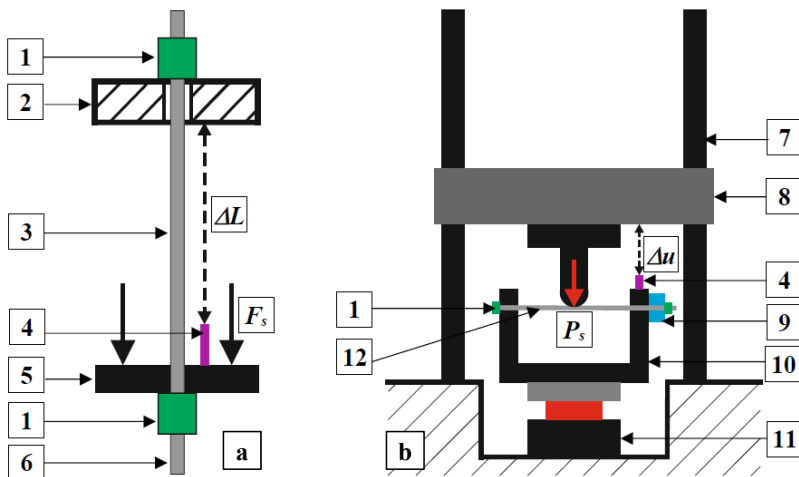

Fig. 3. Test setup for cable bolt and wire rope lacing tests under static loading: a – wire rope loaded by a force applied along its axis, b – wire rope loaded by a force applied perpendicular to its axis; 1 – wire rope barrel and wedge clamp; 2 – fixed crosshead of the ZMLK 500 testing machine; 3 – cable bolt rope; 4 – displacement (bolt rope elongation / deflection) sensor; 5 – moving crosshead loading the wire rope; 6 – cable bolt rope end; 7 – load-bearing post of the AJ AMSLER testing machine; 8 – fixed crosshead with a beam loading the wire rope lacing perpendicularly to the rope axis; 9 – wire rope lacing tensile force sensor; 10 – load-bearing frame of the wire rope lacing testing facility; 11 – hydraulic actuator; 12 – lacing rope

A force distribution diagram for the static load P_s applied perpendicular to the wire rope lacing axis at the centre of its length is presented in Fig. 4a, whereas an analogous force distribution diagram under dynamic loading is presented in Fig. 4b. The tests of wire rope lacing with a rope length $L_0 = 1320$ mm (length between the internal surfaces of the wedges in an MK4 barrel and wedge clamp) under static loading involved measuring the transverse force P_s, the rope tension T_s and deflection u, whereas under dynamic loading: the tension T_d and deflection u. Measurements of the force P_d were omitted during dynamic testing due to the high risk of force sensor damage.

The energy absorbed by the wire rope lacing E_{2s} under static loading P_s (Fig. 4a) until the failure of the first wire is calculated using the following formula:

$$E_{2s} = \int_0^{u_{max}} P_s(u)\,du, \ [\text{kJ}] \tag{2}$$

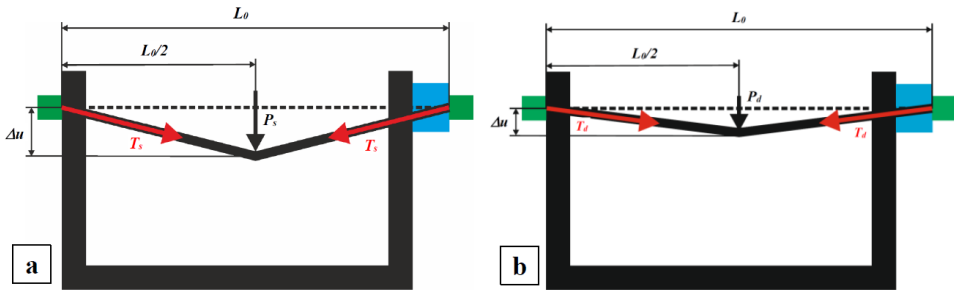where: Δu_{max} – maximum rope deflection at failure, mm.

Fig. 4. Force distribution diagram for loads applied to a wire rope fixed in a testing machine under static (a) and dynamic (b) loading

The formula defined in the relevant standard [56] was applied in order to determine the percentage reduction in the greatest force $P_{s\max}$ obtained during the loading of the wire rope lacing at the centre of its length in a direction perpendicular to its axis (Fig. 3b), relative to the maximum force $F_{s\max}$ loading the rope during tensile testing (Fig. 3a):

$$D_i = \left(1 - \frac{T_{s\max}}{F_{s\max}}\right) \cdot 100, \quad [\%] \tag{3}$$

Additionally, thermal imaging measurements at the contact point of the element loading the wire rope (Fig. 3b) were carried out during the static tensile testing of the wire rope lacing in order to observe the stress distribution at the contact point and to compare it to the temperature distribution in the remaining part of the rope. The tests utilised a Testo 890–1 thermal camera [55], the technical parameters of which are presented in TABLE 2.

TABLE 2

Parameters of the Testo 890–1 infrared camera used during tests

Camera parameter	Value
Infrared resolution	640×480 pixels
Lens	15°×11° Telephoto 15 mm f/0.9
Geometric resolution (IFOV)	0.42 mrad
Thermal sensitivity	<40 mK
Measurement range	−30°C to +100°C
Accuracy	±2% of reading
Emissivity setting	0.95

The cable bolt and wire rope lacing test methodology under impact loading, as developed at the Central Mining Institute (GIG), is based on the drop weight impact method. A test facility with a height $H = 9$ m (the height of the load-bearing posts that also serve to guide the ram) makes it possible to test various structural elements, particularly steel arch, rock bolt and surface support elements under cyclic (impact) loading. A diagram of the test facility with a frame for bolt testing is presented in Fig. 5a, and a frame for rope lacing tests in Fig. 5b, whereas its view is displayed in Photo 1.

Before testing, a cable bolt (Fig. 5a) or wire rope lacing (Fig. 5b), terminated with barrel and wedge clamps at both ends, is subjected to static loading by the mass of a steel crossbeam (known as a crosshead), which, when struck by the ram produces a combined system of two masses that exert dynamic loading on the wire rope, resulting in its tension. The same test frame (Fig. 5b) as during static testing (Fig. 3b) was used for the wire rope lacing tests under impact loading.
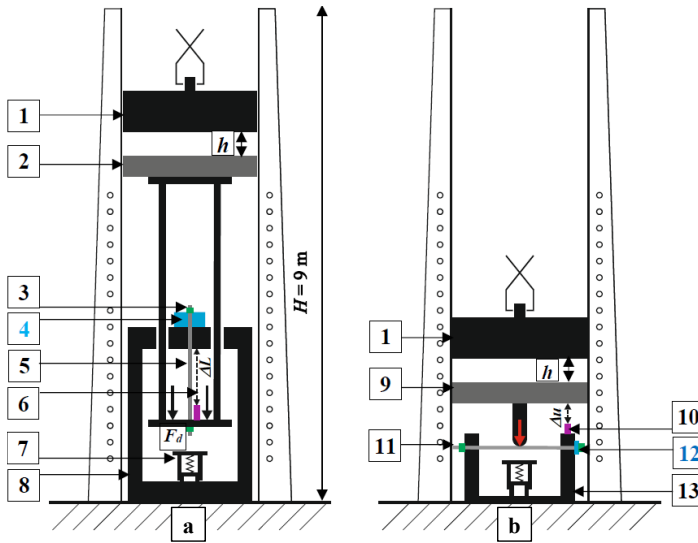

Fig. 5. Test setup for testing cable bolts and wire rope lacing at a 1:1 scale by means of the impact of a free-falling ram mass: a – wire rope loaded by a force applied along its axis, b – wire rope loaded by a force applied perpendicular to its axis; 1 – ram with a mass m; 2 – crossbeam (crosshead) with a mass m_1 applying static loading to the cable bolt; 3 – wire rope barrel and wedge clamp; 4 – sensor for the dynamic tensile force F_d applied to the cable bolt; 5 – cable bolt rope; 6 – displacement (cable bolt elongation $\otimes L$) sensor; 7 – impact energy absorber; 8 – frame for tensile bolt testing; 9 – crosshead applying static loading to the wire rope lacing, perpendicular to its axis; 10 – wire rope displacement / deflection $\otimes u$ sensor; 11 – wire rope lacing; 12 – sensor for the tensile force T_d applied to the wire rope lacing; 13 – frame for wire rope lacing tests under loading perpendicular to the wire rope axis

The frame for tensile bolt testing presented in Fig. 5a makes it possible to test just the bolt bars and ropes by themselves, terminated with a thread or rope clamp on both ends, as well as bolts anchored in test cylinders filled with concrete or a different cement binder imitating rock. The frame enables the simulation of dynamic bolt loading consisting of the sudden application or the free fall of a ram mass of up to 20,000 kg on the crosshead (with a mass of 1600 kg, 3300 kg or 6600 kg) that exerts static loading on the bolt. Tests of the shaft hoist ropes, wire ropes used in pit bottoms [61,62,63], and a chain feeder are conducted by the frame.

The test frame for wire rope lacing tests presented in Fig. 5b enables the testing of not just single wire ropes in a lacing, but also assemblies of combined ropes forming fragments of surface support. The impact mass (ram) is equipped with guides, whose construction prevents the jamming of the ram between the two test facility load-bearing posts, which also serve the function of guide posts.
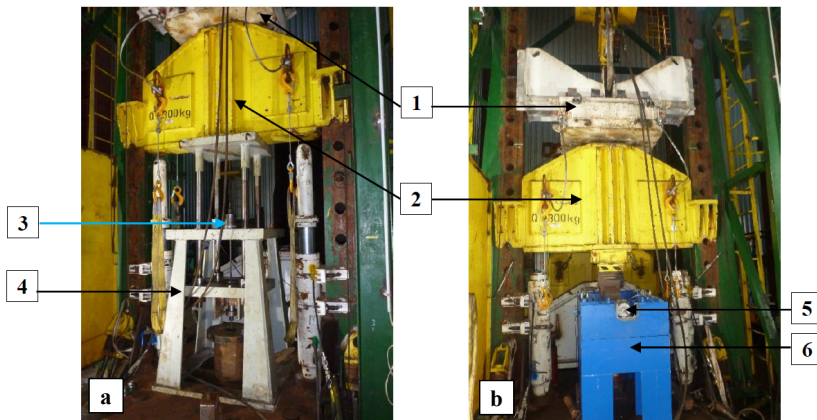
Photo 1. View of the facilities for cable bolt (a) and wire rope lacing (b) tests at real scale: 1 – impact mass (ram) of 4000 kg; 2 – crossbeam (crosshead) with a mass of 3300 kg exerting static loading on the cable bolt or wire rope lacing; 3 – sensor for the tensile force applied to the bolt rope; 4 – facility frame for bolt testing under (tensile) impact loading; 5 – sensor for the tensile force applied to the wire rope lacing; 6 – frame for wire rope lacing tests (rotated by 90° in the facility relative to the setup in Fig. 5)

The primary element of the measuring system, utilised in the dynamic testing at the test facility (Photo 1), was the HBM DMCplus measuring amplifier equipped with 20-bit analogue-digital converters. The amplifier was connected to C6 strain gauge force sensors (HBM, class 0.5) with a measuring range of 2 MN (Fig. 5a) and 500 kN (Fig. 5b) as well as an FT 80 RLA−500 laser displacement sensor (SensoPart) [64] with a resolution of 0.5 mm, measuring range up to 500 mm and non-linearity under 0.25% of the measuring range.

A total of 10 pieces of wire rope with a length $L_0 = 1050$ mm (internal dimension between the barrel and wedge clamps) were subjected to cable bolt testing at cyclic (impact) tensile loading per the load case in Fig. 5a. The tests consisted in the multiple loading (until failure) of the bolt mounted by itself in the test facility by applying a dynamic force by means of the impact of a free falling ram with a mass m against a crosshead with a mass m_1 that exerted static tensile loading on the bolt rope. Parameters measured during the tests included the dynamic tensile force loading the bolt rope F_d as well as the rope elongation ΔL as a function of time t with a sampling frequency $f_s = 9.6$ kHz. The comparative analysis that constitutes the subject of this paper involved tests during which wire rope failure occurred as a result of a single impact.

3 pieces of wire rope with a length $L_0 = 1320$ mm (internal dimension between the barrel and wedge clamps) were subjected to wire rope lacing tests under impact loading P_d perpendicular to the rope axis per the load case in Fig. 5b. Parameters measured during the tests included the dynamic tensile force loading the wire rope lacing T_d as well as the rope deflection Δu as a function of time t with a sampling frequency $f_s = 4.8$ kHz. The lower sampling frequency f_s relative to the cable bolt testing was adopted because the impact velocities during the wire rope lacing tests were considerably lower than during the cable bolt tests.

During testing, at the point of the collision of masses m and m_1 over a single dimension (the motion of both the bodies before and after collision proceeds along a single straight line), no rebound of the masses was observed, which means that a fully inelastic case of mass collision can be adopted for the body velocity and energy calculations [65,66]. Per the law of conservation

of momentum, the velocity v_p of the combined masses m and m_1 after collision can be calculated from the following formula:

$$mv_1 = (m + m_1)v_p \qquad (4)$$

which is used to calculate the value of v_p:

$$v_p = \frac{mv_1}{m + m_1}, \ [\text{m} \cdot \text{s}^{-1}] \qquad (5)$$

where v_1 – impact velocity of a ram with a mass m against a crosshead with a mass m_1, which is calculated using the following formula:

$$v_1 = \sqrt{2gh}, \ [\text{m} \cdot \text{s}^{-1}] \qquad (6)$$

where:
   g – gravitational constant 9.81 [m·s^{-2}],
   h – ram mass free fall height [m].

The energy E_{1d} absorbed by the cable bolt rope (Fig. 5a) until failure is calculated using the following formula:

$$E_{1d} = \int_0^{L_{\max}} F_d(L)\,dL, \ [\text{kJ}] \qquad (7)$$

The energy E_{2d} absorbed by the wire rope lacing (Fig. 5b) until failure, under dynamic loading applied at the centre of its length, perpendicular to its axis, is calculated using the following formula:

$$E_{2d} = E_{2dk} + E_{2dp}, \ [\text{kJ}] \qquad (8)$$

where: E_{2dk} – kinetic impact energy of the combined masses m and m_1 against the wire rope lacing, as calculated using the following formula:

$$E_{2dk} = \frac{(m + m_1)v_p^{\,2}}{2}, \ [\text{kJ}] \qquad (9)$$

E_{2dp} – potential energy resulting from the height change of the combined masses m and m_1 following the wire rope lacing deflection (Fig. 5b) by a value of $u_{\max}$ at wire rope failure, as calculated from the following formula:

$$E_{2dp} = (m + m_1)g \cdot u_{\max}, \ [\text{kJ}] \qquad (10)$$

3. Results and discussion

Fig. 6 presents typical relationship charts of load as a function of wire rope elongation $F_s = f(\Delta L)$ and wire rope tension as a function of strain $\sigma = f(\varepsilon)$ as determined during the tension of Ø15.7 mm cable bolts under static loading (per the load case in Fig. 3a) until the total loss of their load capacity.
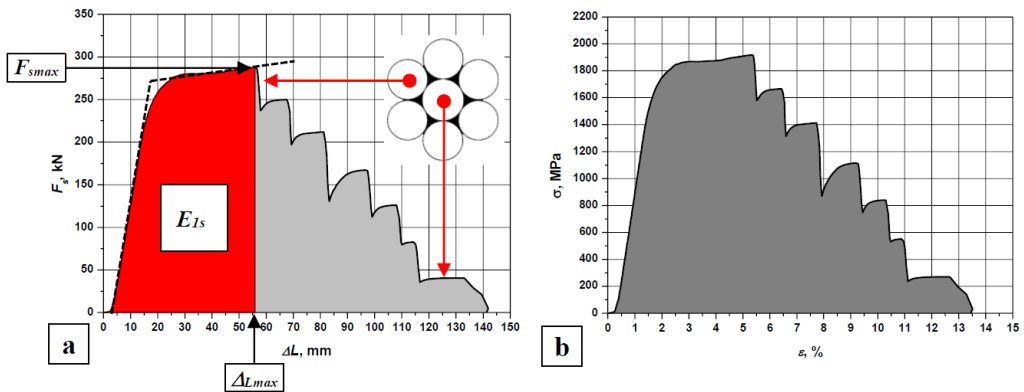
Fig. 6. Typical $F_s = f(\Delta L)$ and $\sigma = f(\varepsilon)$ relationship charts determined during the tensile testing of Ø15.7 mm cable bolts under static loading

The successive loading force decreases in the $F_s = f(\Delta L)$ relationship chart presented in Fig. 6a, whose envelopes are close to a step chart, resulting from rupturing in consecutive strand wires and the core wire. The character of the $F_s = f(\Delta L)$ relationship is similar to the results of tests conducted in other laboratories [51], which investigated the Y1860 – S7 strand load capacity in wedge anchorage. Until the first wire failure, the rope loading course as a function of elongation resembles a bilinear function (dotted polyline), which is used, e.g. during the design of reinforced concrete constructions prestressed by means of wire ropes [48]. It should be noted that the part of the polyline until the rope failure is considerably longer under static loading than under dynamic loading. As a result, under static loading, $D_{L\max} = 56$ mm and under dynamic loading (Fig. 8), $D_{L\max} = 37$ mm. The test results confirmed the high cable bolt rope strength, which considerably exceeds the strength class of 1860 MPa declared by the manufacturer, as presented in TABLE 3 on the example of the charts obtained based on the test in Fig. 6.

TABLE 3

Example mechanical properties of a cable bolt rope, calculated based on the test presented in the form of charts in Fig. 6

A, mm²	$F_{s\max}$, kN	R_m, MPa	$F_{p0.2}$, kN	$R_{p0.2}$, MPa
149.83	287.70	1920.21	252.09	1682.54

where: A – metallic cross-section, R_m – tensile strength, $R_{p0.2}$ – wire rope proof stress, $F_{p0.2}$ – force resulting in cable bolt rope plasticity at $R_{p0.2}$.

A test result compilation in the form of average $F_{s\max}$ and E_{1s} values and their standard deviation is included in TABLE 4.

Breaking force and ultimate stress test results confirmed that the wire ropes fulfil the relevant standard requirements: $F_{\min} = 279.0$ kN for wire ropes intended for prestressed constructions, produced to a strength class $R_m = 1860$ MPa. Wire rope failure occurred at an average force $F_{s\max} = 289.0$ kN. Until the failure of the first wire in the rope, the average energy absorbed by the cable bolt was $E_{1s} = 16.6$ kJ.

TABLE 4

Average values and standard deviation for forces and energy absorbed by cable bolts and wire rope lacing
until failure during testing under static and dynamic loading

Static bolt tension		Dynamic bolt tension		Static wire rope lacing loading by a transverse force			Dynamic wire rope lacing loading by a transverse force	
$F_{s\max}$, kN	E_{1s}, kJ	$F_{d\max}$, kN	E_{1d}, kJ	$P_{s\max}$, kN	$T_{s\max}$, kN	E_{2s}, kJ	$T_{d\max}$, kN	E_{2d}, kJ
289.0 ±11.2	16.6 ±2.7	279.1 ±7.2	8.68 ±0.82	119.2 ±6.7	264.4 ±10.6	4.58 ±0.49	246.4 ±7.1	5.04 ±0.18

Fig. 7 presents typical $P_s = f(\Delta u)$ and $T_s = f(\Delta u)$ relationship charts determined under static loading (per the load case in Fig. 3b and 4a) during the loading of Ø15.7 mm wire rope lacing at the centre of its length, perpendicularly to the longitudinal wire rope axis. A test result compilation in the form of average $P_{s\max}$, $T_{s\max}$ and E_{2s} values and their standard deviation is included in Table 3.
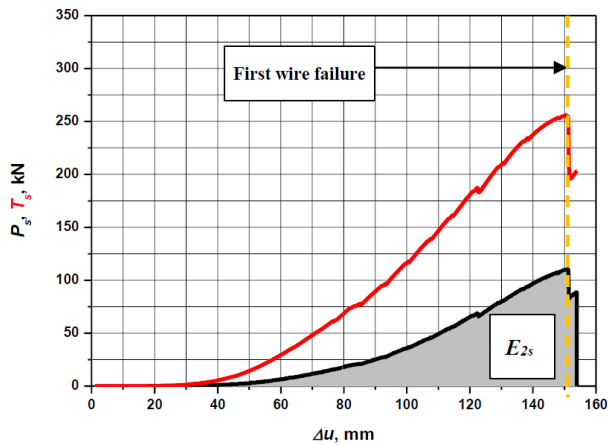

Fig. 7. Typical $P_s = f(\Delta u)$ and $T_s = f(\Delta u)$ relationship charts determined during the testing of Ø15.7 mm wire rope lacing under static loading at the centre of its length, perpendicular to its longitudinal axis

The calculated D_i factor describing the reduction of the maximum force $T_{s\max}$ relative to $F_{s\max}$ is 8.5%. This results primarily from the fact that the rope wires are affected by an additional shearing force P_s, which decreases the rope strength at the contact point with the loading element in the form of a cylinder (as confirmed in thermal images: Photo 2a and Photo 2b). The shearing force also affects the considerable reduction in the energy E_{2s} absorbed by the rope until failure, which, on the example of the chart from the test in Fig. 7, is lower by 72% than the energy E_{1s} absorbed by the rope during tension.

The failure of the first wire in the wire rope lacing occurred at an average maximum loading force $P_{s\max} = 119.2$ kN (Fig. 5a), which generated an average maximum tension $T_{s\max} = 264.4$ kN in the wire rope. Until the failure of the first wire, the average energy absorbed by the wire rope lacing was $E_{2s} = 4.58$ kJ. It should be noted that the relatively minor loading of the wire rope

with a transverse force P_s generated a considerably higher tension T_s in the wire rope. In this case, the tension is 1.3 times greater than the transverse force. It should however be mentioned that the rope was not pre-tensioned during the tests, and the entire rope assembly exhibited certain slack that influenced on the initial wire rope deflection u_0, which in turn affected the value of the T_s / P_s relationship. This phenomenon is often used in measurements to determine rope tension, though on a considerably smaller measurement base and within the boundaries of rope elasticity, but this is not the subject of this paper and will not be discussed in broader detail.

Instead, attention was devoted to the phenomenon occurring at the contact point of the wire rope and the cylinder constituting the testing machine's loading element. Using a thermal camera for the tests made it possible to observe the significant heating of the rope wires at the contact point with the steel cylinder constituting the testing machine's loading element (Fig. 3b), from an initial temperature of 26.9°C to a temperature of 101.9°C at rope wire failure. Thermal images (Photo. 2) present the contact point of the wire rope and the steel cylinder before (Photo 2a) and after (Photo 2b) wire failure.
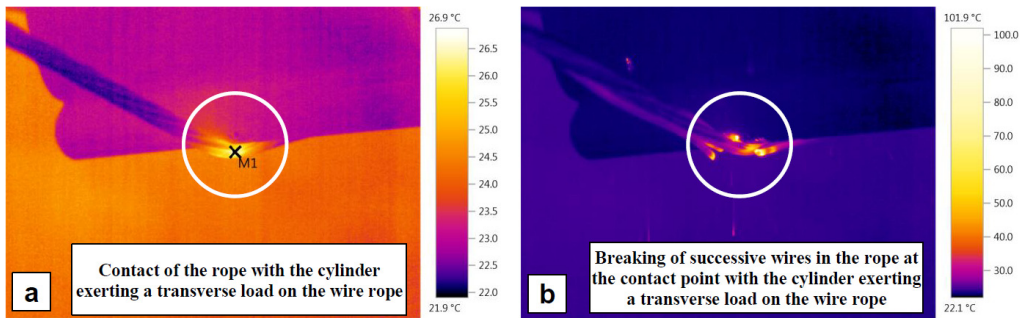

Photo 2. Wire rope tensile testing by deflection with a transverse force toward the rope axis:
a – test commencement; b – wire rope failure as a result of successive strand breaking

The occurrence of increased stress at the contact of the loading element and the wires in the strand, manifesting itself in the significant heating of rope wires within the contact area, can have a negative influence on the reduction of stresses at the contact of the loading element and the rope, which had been observed earlier during the static wire rope lacing tests. Fig. 8 presents a typical relationship chart of loading as a function of wire rope elongation $F_d = f(\Delta L)$ as determined during the tension of the Ø15.7 mm cable bolt under dynamic loading (per the load case in Fig. 5a) until the total loss of its load capacity (breaking of all the wires in the strand). A test result compilation in the form of average $F_{d\max}$ and E_{1d} values and their standard deviation is included in Table 3.

Cable bolt failure under dynamic loading occurred at an impact velocity of the combined ram and crosshead masses ranging within $v_p = 1.4$-1.5 m/s.

A typical course of impact loading by means of a free falling ram with a mass of 4000 kg from a height $h = 0.45$ m (Fig. 8) resulted in a rapid increase of the rope load rate to a maximum value of 32 kN/ms, which is significantly higher than the standard value of 1.395 kN/s [58] for rope load rates under static loading. The wire rope suffered rapid failure over about 25 ms. Such a substantial increase in the load rate certainly intensified the brittle cracking of the wires in the
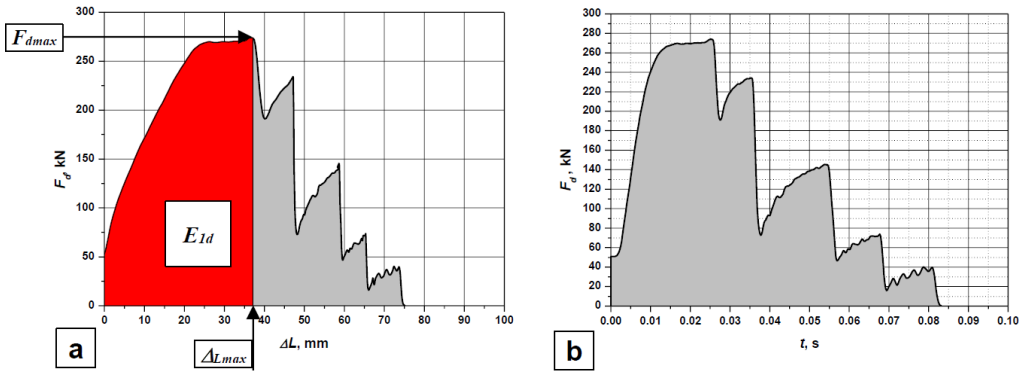
Fig. 8. Typical $F_d = f(\Delta L)$ relationship chart determined during the tension of a Ø15.7 mm cable bolt under dynamic loading

rope, which led to a significant reduction of the energy absorbed by the rope until its failure, to a value of $E_{1d} \approx 8.7$ kJ, as a result of the considerable decrease in the wire rope elongation relative to the static loading (Fig. 6).

The average dynamic force leading to wire rope failure $\boldsymbol{F_{d\,max}} = 279.1$ kN is slightly higher than the minimum static force $\boldsymbol{F_{min}} = 279$ kN defined in the relevant standard, whereas the average energy $\boldsymbol{E_{1d}}$ absorbed by the cable bolt until failure is 48% lower than the energy $\boldsymbol{E_{1s}}$ determined during the Ø15.7 mm wire rope failure under static loading.

Fig. 9 presents a typical relationship chart of wire rope lacing tension as a function of deflection $T_d = f(\Delta u)$ as determined during the dynamic loading of the Ø15.7 mm wire rope lacing with a force P_d perpendicular to the wire rope axis (per the load case in Fig. 5b) until the total loss of its load capacity. A test result compilation in the form of average $T_{d\,max}$ and E_{2d} values and their standard deviation is included in Table 3.

Wire rope lacing failure under dynamic loading occurred at an impact velocity of the combined ram and crosshead masses ranging within $\boldsymbol{v_p} = 0.55$-0.77 m/s.
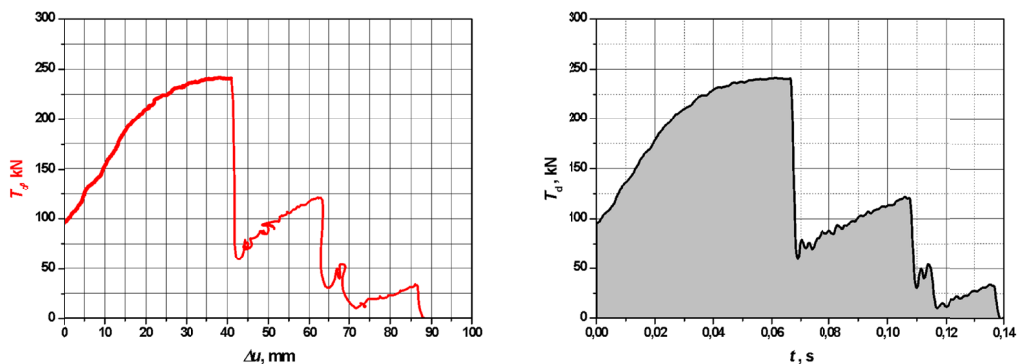

Fig. 9. Typical relationship chart of wire rope lacing tension as a function of deflection $T_d = f(\Delta u)$ as determined during the dynamic loading of Ø15.7 mm wire rope lacing with a force P_d perpendicular to the wire rope axis

A typical course of impact loading perpendicular to the wire rope by means of a free falling ram with a mass of 4000 kg from a height $h = 0.10$ m (Fig. 9) led to a slower rope load rate increase – to a maximum of 7.5 kN/ms – relative to the 32 kN/ms under axial tensile loading (Fig. 8). Despite that, the wire rope also suffered rapid failure over about 60 ms. Such a quick failure of the wire rope was influenced by both the shearing force P_d and the brittle cracking of the wires forming the rope. These factors also had an effect on the low energy $E_{2d} \approx 5$ kJ absorbed by the wire rope, which was comparable to the energy $E_{2s} \approx 4.5$ kJ obtained under static transverse loading.

The average dynamic tension at wire rope lacing failure was $T_{d\max} = 246.4$ kN, which is lower by 7% compared to $T_{s\max}$. The dynamic influence of the force at the contact of the loading element and the wire rope, which results in brittle cracking, is the most likely cause of the negative effect on this phenomenon.

4. Conclusions

This paper attempts to supplement a certain research gap concerning the determination of the manner in which static and dynamic loads perpendicular to the axis of the wire rope lacing affect its strength. The novelty of the paper also lies in the strength comparison of the ropes subjected to tension as well as the ropes loaded transversely to their axis of symmetry.

The greatest values of breaking force and energy absorbed until failure for the Ø15.7 mm wire rope were found for ropes tested under static tensile loading: $F_{s\max} = 289.0 \pm 11.2$ kN and $E_{1s} = 16.6 \pm 2.7$ kJ.

A comparative test result analysis for the wire ropes used in the bolt designs revealed that the influence of dynamic loading forces has a significant effect on reducing the rope load capacity, which results in the brittle cracking of the wires in the rope. Although the average dynamic force leading to wire rope failure $F_{d\max} = 279.1$ kN is comparable to the minimum static force $F_{\min} = 279$ kN defined in the relevant standard, the average energy E_{1d} absorbed by the cable bolt until failure is **48% lower** than the energy E_{1s} determined for wire rope failure under static loading. Furthermore, cable bolt failure under dynamic loading occurred at an impact velocity of the combined ram and crosshead masses ranging within $v_p = 1.4$-1.5 m/s.

It was also found that in the case of wire ropes used as lacing supporting the operation of wire mesh, their load capacity also undergoes reduction following the generation of additional stresses resulting from loading perpendicular to the wire rope axis, as confirmed by thermal imaging. The temperature during wire failure under static loading exceeded 100°C, which indicates high contact stress at the contact point of the rope and the loading element simulating the load exerted by the rock mass.

The experience obtained from the conducted tests enables the formulation of a conclusion that given the high strength and low yield of the wire ropes, they are intended primarily for assuming dynamic loads characterised by minor impact energy and velocity. Therefore, according to our assessment, the ropes should be applied in rigid rock bolt support, where the wire rope is required to exhibit a high load capacity and low yield.

The wire rope lacing, operating at minor slack and with no pre-tensioning, reinforces surface support assemblies formed from steel mesh, which prevents the intrusion of rock into a working. However, contact with sharp rock edges should be avoided, as it generates additional stress at the contact point with the rope wires and reduces the rope load capacity.

The cable bolt tests will be continued using various load cases and impact velocities in order to inspect the possibility of increasing the wire rope yield, which would enable the absorption of greater impact energies by the ropes.

Acknowledgements

References

[1] M. Cała, J. Flisiak, A. Tajduś, Mechanizm współpracy kotwi z górotworem o zróżnicowanej budowie, Biblioteka Szkoły Eksploatacji Podziemnej, Seria z Lampką Górniczą, nr 8, 2001 Instytut Gospodarki Surowcami Mineralnymi i Energią PAN, Kraków (in Polish).

[2] L.O. Dzakir, M.A. Rai, N.P. Widodo: Analysis of Reinforcement System (Rock Bolt and Shotcrete) Effect on The Pillars Strength in Underground Mining Using Physical Models Testing in Laboratory. Jurnal Geomine **9** (1), 73-87 (2021).

[3] A. Kidybiński, A. Nierobisz, Obudowa kotwiowo-cięgnowa (OK-C) jako alternatywa obudowy ŁP. Przegląd Górniczy **64** (11-12), 7-13 (in Polish) (2008).

[4] W. Korzeniowski, K. Skrzypkowski, Ł. Herezy, Laboratory Method for Evaluating the Characteristics of Expansion Rock Bolts Subjected to Axial Tension. Archives of Mining Sciences **60** (1), 209-224 (2015).

[5] O. Krykovskyi, V. Krykovska, S. Skipochka, Interaction of rock-bolt supports while weak rock reinforcing by means of injection rock bolts. Mining of Mineral Deposits **15** (4), 8-14 (2021).

[6] C.C. Li, Field Observations of Rock Bolts in High Stress Rock Masses. Rock Mechanics and Rock Engineering **43**, 491-496 (2010).

[7] C.C. Li, Rockbolting. Principles and Applications, 2017 Oxford, Butterworth-Heinemann.

[8] C.C. Li, Principles of Rockbolting Design. Journal of Rock Mechanics and Geotechnical Engineering **9** (3), 396-414 (2017).

[9] C.C. Li, Principles and Methods of Rock Support for Rockburst Control. Journal of Rock Mechanics and Geotechnical Engineering **13** (1), 46-59 (2021).

[10] C.C. Li, G. Stjern, A. Myrvang, A Review on the Performance of Conventional and Energy-Absorbing Rockbolts. Journal of Rock Mechanics and Geotechnical Engineering. **6** (4), 315-327 (2014).

[11] C.C. Li, J. Hadjigeorgiou, P. Mikula, G. Knox, B. Darlington, R. Royer, A. Pytlik, M. Hosp, Performance of Identical Rockbolts Tested on Four Dynamic Testing Rigs Employing the Direct Impact Method. Journal of Rock Mechanics and Geotechnical Engineering **13** (4), 745-754 (2021).

[12] A. Nierobisz, Analiza wpływu obciążeń dynamicznych na zachowanie się kotwi. Prace Naukowe Głównego Instytutu Górnictwa. Górnictwo i Środowisko **2**, 79-105 (in Polish) (2004).

[13] A. Nierobisz, The Model of Dynamic Loading of Rockbolts. Archives of Mining Sciences **51** (3), 453-470 (2006).

[14] A. Nierobisz, Analiza badań odporności dynamicznej elementów i zespołów obudów górniczych. 2008 Główny Instytut Górnictwa, Katowice (in Polish).

[15] A. Nierobisz, Rola obudowy w utrzymywaniu wyrobisk korytarzowych w warunkach zagrożenia tąpaniami. Prace Naukowe Głównego Instytutu Górnictwa. Studia, Rozprawy, Monografie, nr 887, 2012 Główny Instytut Górnictwa, Katowice (in Polish).

[16] A. Nierobisz, Z. Barecki, Zastosowanie obudowy kotwowo-cięgnowej i cięgłowej. Przegląd Górniczy **69** (7), 14-27 (in Polish) (2013).

[17] W. Podgórski, K. Podgórski, Obudowa kotwiowa wyrobisk górniczych, 1969 Wydawnictwo Śląsk, Katowice (in Polish).

[18] W. Pytel, Geomechaniczne problemy doboru obudowy kotwowej dla wyrobisk górniczych, 2012 KGHM CUPRUM – Centrum Badawczo-Rozwojowe, Wrocław (in Polish).

[19] A. Pytlik, Comparative Shear Tests of Bolt Rods Under Static and Dynamic Loading. Studia Geotechnica et Mechanica **42** (2), 151-167 (2020).

[20] A. Pytlik, Odporność udarowa kotew górniczych, 2022 Główny Instytut Górnictwa, Katowice (in Polish).

[21] A. Pytlik, S. Prusek, W. Masny, Methodology for Laboratory Testing of Rockbolts Used in Underground Mines Under Dynamic Loading Conditions. Journal of the Southern African Institute of Mining and Metallurgy **116** (12), 1101-1110 (2016).

[22] K. Skrzypkowski, Laboratory Testing of a Long Expansion Rock Bolt Support for Energy-Absorbing Applications. In E3S Web of Conferences. 17th Conference of PhD Students and Young Scientists, 23-26 May 2017, Szklarska Poręba (**29**, 00004). Les Ulis, EDP Sciences (2018).

[23] K. Skrzypkowski Evaluation of Rock Bolt Support for Polish Hard Rock Mines. In E3S Web of Conferences. Scientific-Research Cooperation Between Vietnam and Poland (POL-VIET 2017), 20-22 November 2018, Kraków (**35**, 01006). Les Ulis, EDP Sciences (2018).

[24] K. Skrzypkowski, W. Korzeniowski, K. Zagórski, P. Dudek, Application of Long Expansion Rock Bolt Support in the Underground Mines of Legnica-Głogów Copper District. Studia Geotechnica et Mechanica **39** (3), 47-57 (2017).

[25] K. Skrzypkowski, W. Korzeniowski, K. Zagórski, I. Dominik, K. Lalik, Fast, Non-Destructive Measurement of Roof-Bolt Loads. Studia Geotechnica et Mechanica **41** (2), 93-101 (2019).

[26] F. Tahmasebinia, A. Yang, P. Feghali, K. Skrzypkowski, Structural Evaluation of Cable Bolts under Static Loading. Applied Sciences **13** (3), 1326 (2023).

[27] N. Tshitema, D.V.V. Kallon, Product Development of a Rock Reinforcing Bolt for Underground Hard Rock Mining. Mining **1** (3), 364-390 (2021).

[28] M. Chudek, Obudowa wyrobisk górniczych. Cz. 1. Obudowa wyrobisk korytarzowych i komorowych, 1986 Wydawnictwo Śląsk, Katowice.

[29] P. Horyl, R. Šňupárek, Behaviour of Steel Arch Supports Under Dynamic Effects of Rockbursts. Mining Technology **116** (3), 119-128 (2007).

[30] M. Turek, Podstawy podziemnej eksploatacji pokładów węgla kamiennego, 2010 Główny Instytut Górnictwa, Katowice (in Polish).

[31] M. Turek (Ed.), Bezpieczeństwo obudowy podporowo-kotwowej w warunkach występowania wstrząsów górotworu, 2012 Główny Instytut Górnictwa, Katowice (in Polish).

[32] M. Turek, S. Prusek, W. Masny, Obudowa podporowo-kotwowa w kopalniach węgla kamiennego, 2015 Główny Instytut Górnictwa, Katowice (in Polish).

[33] T. Majcherczyk, Z. Niedbalski, P. Małkowski, Ł. Bednarek, Analysis of Yielding Steel Arch Support with Rock Bolts in Mine Roadways Stability Aspect. Archives of Mining Sciences **59** (3), 641-654 (2014).

[34] Y. Zhao, N. Liu, X. Zheng, N. Zhang, Mechanical Model for Controlling Floor Heave in Deep Roadways with U-Shaped Steel Closed Support. International Journal of Mining Science and Technology **25** (5), 713-720 (2015).

[35] A. Pytlik, Comparative Bench Testing of Steel Arch Support Systems with and without Rock Bolt Reinforcements. Archives of Mining Sciences **64** (4), 747-764 (2019).

[36] A. Pytlik, Tests of Steel Arch and Rock Bolt Support Resistance to Static and Dynamic Loading Induced by Suspended Monorail Transportation. Studia Geotechnica et Mechanica **41** (2), 81-92 (2019).

[37] A. Pytlik, Experimental Studies of Static and Dynamic Steel Arch Support Load Capacity and Sliding Joint Temperature Parameters During Yielding. Archives of Mining Sciences **65** (3), 469-491 (2020).

[38] X. Sun, L. Wang, Y. Lu, B. Jiang, Z. Li, J. Zhang, A Yielding Bolt – Grouting Support Design for a Soft-Rock Roadway Under High Stress. A Case Study of the Yuandian no. 2 Coal Mine in China. Journal of the Southern African Institute of Mining and Metallurgy **118**, 71-82 (2018).

[39] W.D. Ortlepp, T.R. Stacey, Final Project Report. Testing of Tunnel Support. Dynamic Load Testing of Rock Support Containment Systems. SIMRAC GAP Project 221. Johannesburg, Safety in Mines Research Advisory Committee (1997).

[40] W.D. Ortlepp, T.R. Stacey, Dynamic Loading of Rockbolt Elements to Provide Data for Safer Support Design. SIMRAC GAP Project 423. Johannesburg, Safety in Mines Research Advisory Committee (1998).

[41] P.K. Kaiser, M. Cai, Design of Rock Support System Under Rockburst Condition. Journal of Rock Mechanics and Geotechnical Engineering **4** (3), 215-227 (2012).

[42] Z. Rak, J. Stasica, Z. Burtan, Skuteczne rozwiązania w systemie wysokiego kotwienia dla wzmacniania obudowy podporowej. Zeszyty Naukowe Instytutu Gospodarki Surowcami Mineralnymi PAN **101**, 101-116 (2017).

[43] M. Cała, A. Roth, Możliwości zastosowania siatek stalowych w warunkach zagrożeń dynamicznych. Górnictwo i Geoinżynieria, R. **31**, 125-133 (2007).

[44] F. Eriksson, Assessment of static performance of LKAB's welded mesh: Laboratory testing and analysis. Civil Engineering, master's level 2020. Luleå University of Technology, Department of Civil, Environmental and Natural Resources Engineering, p. 95 (2020). http://www.diva-portal.org/smash/get/diva2:1381608/FULLTEXT02.pdf

[45] Y. Potvin, D. Heal, Dynamic testing of high energy absorption (HEA) mesh. In Proc 5th Int. Seminar on Deep and High Stress Mining, Santiago, Australian Centre for Geomechanics, 283-300, (2010).

[46] Y. Potvin, J. Wesseloo, D. Heal, An Interpretation of Ground Support Capacity Submitted to Dynamic Loading. Mining Technology **119** (4), 233-245, (2010).

[47] A. Pytlik, Graniczne wartości obciążenia dynamicznego powodujące niszczenie okładzin górniczych. Przegląd Górniczy **71** (5), 78-84, (2015).

[48] J.C. Carroll, T.E. Cousins, C. L. Roberts-Wollmann, The use of Grade 300 prestressing strand in pretensioned, prestressed concrete beams. Precast/Prestressed Concrete Institute (PCI), PCI Journal **62** (1), 49-65 (2017).

[49] E. Villaescusa, Ground Support Research at the WA School of Mines. International Journal of the Japanese Committee for Rock Mechanics **5** (1), 1-10, (2009).

[50] PN-G-15050:2018-01: Obudowa wyrobisk górniczych – Siatki okładzinowe zgrzewane (in Polish) (2018).

[51] J. Kubiak, A. Łodo, J. Michałek, Badania nośności splotów typu Y1860-S7 w zakotwieniach szczękowych. Materiały Budowlane **3**, 35-37, (in Polish) (2013).

[52] ASTM F432-19: Standard Specification for Roof and Rock Bolts and Accessories (2019).

[53] CAN/CSA-M430-90: Roof and Rock Bolts, and Accessories (1990).

[54] Z. Dyląg, A. Jakubowicz, Z. Orłoś, Wytrzymałość materiałów tom II. Podręczniki Akademickie. Mechanika, 1997 Wydawnictwo Naukowo-Techniczne (in Polish).

[55] P. Szade, M. Szot, B. Kubiś, Thermoelastic effect in compacted steel wire ropes under uniaxial loading. Quantitative InfraRed Thermography Journal **18** (4), 252-268 (2021).

[56] ISO 15630-3: Steel for the reinforcement and prestressing of concrete – Test methods – Part 3: Prestressing steel (2019).

[57] prEN 10138-3:2006: Prestressing steels – Part 3: Strand (2006).

[58] EN 12385-1:2002+A1: Steel wire ropes – Safety – Part 1: General requirements (2008).

[59] M.C. Girona, M.C. Verge, G.R. Rodriguez, Á.C.A. Bengoechea, Optimización de placas de anclaje y empalme mediante modelos numéricos de elementos finitos. V Congreso de la Asociación Cientificotecnica del Hormigón Estructural (ACHE). Del 25 al 27 de OCTUBRE de 2011, Barcelona. 1-10 (2011).

[60] cB. Markocki, S. Makar, R. Rogowski, Wybrane problemy w realizacji konstrukcji wstęgowej z betonu sprężonego na podstawie kładki pieszo-jezdnej w miejscowości Lubień. Przegląd Budowlany **84** (1), 40-45 (2013).

[61] P. Gospodarczyk, Computer simulation usage for verification of deepened shaft artificial bottom construction. Archives of Mining Sciences **60** (4) (2015).

[62] P. Gospodarczyk, G. Stopka, M. Szot, Innowacyjne rozwiązanie sztucznego dna szybu dla kopalni Jankowice. Przegląd Górniczy **72** (6), 78-84 (2016).

[63] M. Szot et al., Patent nr PL 397064. Artificial bottom of the shaft platform.

[64] A. Szade, M. Szot, A. Ramowski, Measurements of rope elongation or deflection in impact destructive testing. Journal of Sustainable Mining **14** (4), 211-218 (2015).

[65] D. Halliday, R. Resnick, J. Walker, Podstawy Fizyki. T. 1., 2007, Wydawnictwo Naukowe PWN, Warszawa (in Polish).

[66] D. Halliday, R. Resnick, J. Walker, Podstawy Fizyki. T. 2., 2008, Wydawnictwo Naukowe PWN, Warszawa (in Polish).